View metadata, citation and similar papers at core.ac.uk

brought to you by CORE

provided by University of Queensland eSpace

Accepted Manuscript

Interfacial energy release rates of SiN/GaAs film/substrate systems determined using a cyclic loading dual-indentation method

Mingyuan Lu, Han Huang

PII: S0040-6090(15)00693-8
DOI: doi: 10.1016/j.tsf.2015.07.027
Reference: TSF 34485

To appear in: *Thin Solid Films*

Received date: 6 October 2014
Revised date: 2 June 2015
Accepted date: 16 July 2015

Please cite this article as: Mingyuan Lu, Han Huang, Interfacial energy release rates of SiN/GaAs film/substrate systems determined using a cyclic loading dual-indentation method, *Thin Solid Films* (2015), doi: 10.1016/j.tsf.2015.07.027

This is a PDF file of an unedited manuscript that has been accepted for publication. As a service to our customers we are providing this early version of the manuscript. The manuscript will undergo copyediting, typesetting, and review of the resulting proof before it is published in its final form. Please note that during the production process errors may be discovered which could affect the content, and all legal disclaimers that apply to the journal pertain.

ACCEPTED MANUSCRIPT

Interfacial energy release rates of SiN/GaAs film/substrate systems determined using a cyclic loading dual-indentation method

Mingyuan Lu, Han Huang*

School of Mechanical and Mining Engineering, The University of Queensland, QLD 4072, Australia

*Corresponding author: han.huang@uq.edu.au

Abstract

Our previous study developed a dual-indentation method for testing the interfacial energy release rate, G_{in}, of the SiN/GaAs film/substrate systems. However, for the film/substrate systems with relatively high interfacial toughness, the dual-indentation method was unable to generate interfacial delamination. In this study, a cyclic loading dual-indentation method was proposed, in which the first monotonic loading in the dual-indentation method was replaced by cyclic loading. It was demonstrated that cyclic loading was effective at inducing delamination in relatively "tough" SiN/GaAs interfaces that were unable to be delaminated by dual-indentation method. The G_{in} values obtained from the cyclic loading indentation were in good agreement with those obtained from the dual-indentation method for the less tough interfaces. The delamination mechanism in the cyclic loading indentation was attributed to the hardening effect on the films induced by cyclic loading, permitting sufficient elastic strain energy to be accumulated to initiate the delamination.

***Key words**: Nanoindentation; delamination; cyclic loading; energy release rate*

ACCEPTED MANUSCRIPT

1 Introduction

The assessment of the adhesion properties of a thin film is imperative to ensure the reliability of the film/substrate system over its life cycles [1]. As a consequence, there is an increasing demand for developing reliable techniques to measure the interfacial adhesion between a film and a substrate. In the past few decades, significant research effort has been directed towards developing approaches to evaluate the adhesion property [1-7]. Among the available techniques, indentation enables the investigation of interfacial adhesion of a film/substrate system to be undertaken in a controllable manner by generating interfacial cracks on a sufficiently small scale and at a specific site [8].

In our previous work, a dual-indentation method was developed to assess the interfacial adhesion of SiN/GaAs film/substrate systems [9]. This method was successfully applied to the SiN/GaAs film/substrate systems with different interfacial properties. The limitation of the dual-indentation approach was that interfacial delamination must be induced during the first indentation. For some SiN/GaAs systems, however, the SiN films did not detach from the GaAs substrate during the first indentation, as the residual elastic strain energy was insufficiently great to induce delamination.

To detach a well-adhered film from a substrate, two techniques were often used. One was to deposit a thick super-layer on top of the film of interest [6, 10]. The super-layer was capable of storing large amount of residual stress and thus provided additional driving force for initiating interfacial delamination without altering the properties of the interface [11]. This method required additional sample preparation, which involved adjusting the thickness and the residual stress of the super-layer so that controlled delamination occurs [1]. The alternative approach was to use cyclic indentation [12-15], during which indentation cycles was done repeatedly at a given load. The interfacial delamination was initiated by the

ACCEPTED MANUSCRIPT

progress of plastic deformation zone in both the film and substrate during each indenting cycle. Compared to the super-layer method, the cyclic indentation method is more controllable and does not require supplementary sample preparation, although the additional plastic deformation resulted from cyclic indentation may potentially weaken the interface through fatigue degradation.

In this study, we used a gradually increasing cyclic loading in the first nanoindentation process, rather than constant cyclic loading [12-15], aiming to minimise the effect of fatigue degradation. The cyclic loading indentation was then followed by a normal nanoindentation, which was thus named as cycle-loading dual-indentation. The developed approach was used to assess the interfacial energy release rate of the well-adhered SiN/GaAs film/substrate systems. `

2 Experimental details

2.1 Specimen

Fifteen SiN/GaAs specimens used in this study were provided by WIN Semiconductors Co. The SiN films were deposited using plasma-enhanced chemical vapour deposition (PECVD) on GaAs (001) substrates using two different PECVD deposition systems, made by Trikon and Novellus, respectively. The deposition was performed in the gaseous mixture of nitrogen, SiN_4 and NH_3. Five types of films deposited using different process conditions were tested, namely Standard SiN, Compressive SiN, DL-com SiN, Dense SiN and Cap SiN. The detailed deposition conditions of the SiN films are shown in Table 1. All the SiN films were characterised by electron diffraction (ED) and their structures were shown to be amorphous [16].

ACCEPTED MANUSCRIPT

2.2 Nanoindentation

Nanoindentation tests were performed at room temperature using a TI900 Hysitron Triboindenter, which is equipped with an *in situ* atomic force microscope (AFM). A Berkovich indenter with an included angle of 142.3° and a tip radius of 100 nm was first used to measure the elastic modulus (*E*) and hardness (*H*) of GaAs substrate and SiN films using the *Oliver-Pharr* method [17]. The *E* and *H* of the films were calculated from *P-h* curves of the film/substrate specimens applying a deconvolution method [18-20]. The values of *E* and *H* are shown in Table 2. It should be noted that interfacial delamination occurred at the near end of the indentation unloading [9, 16, 21], marked by the pop-out event, and only the initial unloading curve was used for characterizing *E* and *H*. The delamination would not affect the initial unloading curve, hence no influence on the calculation of *E* and *H*.

For the adhesion measurement a conical indenter with spherical apex that has an included angle of 120° and a tip radius of 3 μm was used. The load function of the cyclic loading dual-indentation is shown in Fig. 1(a). The loading process of the first indentation was composed of 33 cycles of loading-unloading with incremental increase of applied load and 50% partial unloading from cycle to cycle. The total time of the cyclic loading process was minimized to reduce the time-dependent creep behaviour in the GaAs substrate. Furthermore, a holding period at each load increment allowed both the instrument and specimen to stabilize. Based on the above considerations, the loading, holding and unloading times of each cycle were set to be 1 second. The unloading of the cyclic loading indentation ceased when the load reached 0.01 mN, so the contact between the indenter and the SiN film could be maintained. After the cyclic indention, a second indentation with loading period of 5 seconds, holding period of 1 second and unloading of 5 seconds was performed. An intermediate holding period of 1 second was applied prior to the second indentation to attenuate the hysteresis in the elastic recovery of the film. The indentation maximum load was varied from 0.5 to 28 mN and

ACCEPTED MANUSCRIPT

different load ranges were applied depending on the thicknesses of the SiN films. For comparison, monotonic loading dual-indentations were also conducted. The load function of a monotonic loading dual-indentation is shown in Fig. 1(b).

3 Cyclic loading indentation Method

As mentioned in our previous study [9], the measurement of G_{in} was based on that the delamination occuring during an indentation process without the occurrence of any film fracture. For some film/substrate systems of relatively strong interfacial adhesion, normal indentation could not induce interfacial delamination. In this case, cyclic loading indentation had to be used. As shown in Fig. 2, cyclic loading was used to replace the first monotonic loading in the dual-indentation method, so well-adhered films could be detached from the substrate.

In the cyclic loading dual-indentation method, the approach that is used to estimate the energy released during delamination and the delaminated area is adopted from that developed in [9]. To obtained the energy released from delamination, U_s, the Griffith energy balance concept is employed to analyse the energy equilibrium in an interfacial delamination event, which can be expressed as [22-24]

$$U = -U_e + U_s + W_d \tag{1}$$

where U_e is the strain energy stored in the flexed film section that detached from the substrate, and W_d is the external mechanical work done by the indenter. To obtain the thermodynamic equilibrium by balancing the all three energy terms, it is required that [24]

$$U = 0 \tag{2}$$

ACCEPTED MANUSCRIPT

Rearranging Eq. (1), we obtain the energy required to generate the interfacial crack surface, written as

$$U_s = U_e - W_d \tag{3}$$

Fig. 3 shows how the energy used for delamination can be obtained from a *P-h* curve of the dual-indentation. Curve OC' is the loading curve of the second indentation and is in fact the response of the elastic bending of the detached film prior to contact with the substrate. Therefore, the area underneath the curve OC', i.e. the area enclosed by OC'CC"O, is the stored elastic strain energy of the deflected film at $h=h_c$. The equivalent mechanical work W_d by the indenter can be calculated by integrating the unloading section over the corresponding displacement range of *ho-hc*, i.e. the area enclosed by OABCC"O. Therefore, according to Eq. (3), the surface energy U_s can be obtained by calculating the area enclosed by OC'CBAO.

To calculate the delamination area, the detached film structure is approximated as a clamped circular plate, as shown in Fig. 4. The delamination area can then be estimated based on the deflection of the clamped circular plate using the circular plate deflexion rule [25]. In this model, the indentation is treated as uniformly distributed load at a concentric circular area of a radius of *b*,

$$b = \left[R_i^2 + \left(R_i - h_c \right)^2 \right]^{1/2} \tag{4}$$

where R_i is the radius of the indenter (R_i=3 μm) and h_c is the contact depth for an typical spherical contact [17], determined by

$$h_c = h - \frac{0.72P}{dP/dh} \tag{5}$$

ACCEPTED MANUSCRIPT

The radius of the delamination area a is associated with the deflection ω of the suspending film, written as [25]

$$\omega = \frac{P_0 b^2 \left(a^2 - 0.75b^2 + b^2 \ln(b/a)\right)}{16D} \quad (6)$$

where P_0 is the load intensity and D is the flexural rigidity of the plate, expressed as

$$P_0 = \frac{P}{2\pi b^2} \quad (7)$$

$$D = \frac{Et^3}{12\left(1-\upsilon^2\right)} \quad (8)$$

where, E, t and υ are the elastic modulus, the thickness and the Poisson's ratio of the film, respectively.

A typical P-h curve of the cyclic-loading dual-indentation is shown in Fig. 5(a). Fig. 5(b) shows the enlarged area marked by the rectangle in dashed line in Fig. 5(a), which is the area of interest for calculating the delamination energy. The loading curve of the 2nd indentation was used to compute the delamination energy release (U_s) and the area being detached from the substrate or the delaminated area (A). The curve in fact includes the responses of the detached film to elastic bending followed by the elastic deformation of both SiN film and GaAs substrate. Thus, it is essential to identify the point of gradient discontinuity, at which the detached film completes the deflection or regains contact with the substrate, in order to accurately obtain U_s and A. Mathematically, the second derivative of the curve, i.e. d^2P/dh^2 in this case, will have a cusp at the gradient discontinuity point. For this purpose, the second derivative, d^2P/dh^2, of the loading curve was calculated and the d^2P/dh^2 is also plotted in Fig. 5(b), where Gaussian smoothing operation was carried out to remove the noise. The apex

ACCEPTED MANUSCRIPT

(Point C') of the d^2P/dh^2 curve indicates the transition point of two distinct stages during the 2nd indentation loading, before which the delaminated film is elastically deflected (Stage I) and after which both the film and substrate are under elastic deformation as an integrated body (Stage II).

In Fig. 5(b), it is clear that the *P-h* curve in Stage II overlaps the unloading curve of the 1st indentation. Both curves can be fitted using the same Hertz elastic contact function (blue lines in Fig. 5(b)). This suggests that the elastic deflection in the 2nd indentation commencing from C' is reversible. In summary, apart from the replacement of the monotonic loading with the cyclic loading, all the deformation and delamination characteristics are the same for these two methods. Thus, the energy model and the circular plate model developed for the monotonic loading dual-indentation [9] can be applied into the calculation of the energy release and delaminated area caused by the cyclic loading dual-indentation. With U_s and A known, the energy release rate, G_{in}, can be calculated by

$$G_{in} = U_s / A \tag{9}$$

Cyclic loading dual-indentation was performed on the film/substrate systems, Compressive and DL-com SiN, to validate this method. The interfacial adhesion of those systems was relatively weak, so the G_{in} values were previously tested using the monotonic loading dual-indentations and were reported in [9]. The G_{in} values obtained from both methods are compared in Table 3, which are in good agreement.

The effect of loading cycles on the calculated G_{in} values was also investigated. For this purpose, cyclic loading dual-indentations with different numbers of cycles were carried out on Compressive SiN specimens. The cycle number varied from 1 to 50. As an example, Fig. 6 shows the G_{in} values obtained from the cyclic loading dual-indentation testing on the 222 nm Compressive SiN film. It appears that the calculated mean values of G_{in} (within 2.1-2.6

ACCEPTED MANUSCRIPT

J/m^2) exhibit no significant variation with the number of cycles. The overall mean G_{in} value is 2.34 J/m^2 and standard deviation is 0.12 (5.3 % of the mean G_{in}). The results demonstrates that the number of cycles had insignificant influence on the calculated G_{in} values.

4 Result

Both monotonic loading and cyclic loading indentations were performed on Standard SiN films to study their deformation behaviours under the two different methods. Fig. 7 shows the *P-h* curves obtained from the indentations on the Standard SiN film of 182 nm in thickness. It is seen that pop-in event occurs during loading in both indentations, which signifies the occurrence of plane slip in GaAs substrate [16]. However, from the *P-h* curve of the monotonic loading indentation, no pop-out is observed during unloading. In contrast, the *P-h* curve of the cyclic loading indentation shows a significant pop-out event. Our previous study [9, 16, 21] clearly demonstrated that a pop-out event at the near end of the unloading process indicated the occurrence of interfacial delamination. Thus, the cyclic loading indentation could initiate interfacial delamination in the film/substrate systems, in which the monotonic loading indentation failed to do so.

Fig. 8 shows the occurrence of delamination events in a group of 18 indentations made using the cyclic loading indentations with different cycle numbers. It is seen in Fig. 8 that the percentage of delamination occurrence increases with the increase in cycle number. When the cycle number is greater than 25, more than 50% of the indentations induce interfacial delamination.

The values of U_s and G_{in} of the Standard SiN films obtained from the cyclic loading indentation are shown in Fig. 9(a) and (b) respectively. U_s appears to increase when the

ACCEPTED MANUSCRIPT

indentation depth is greater, because higher penetration generates larger delamination area, therefore higher surface energy released. In Fig. 9(b), the G_{in} values are plotted as a function of the indentation depth too. It is seen that for a specific film/substrate system the values of G_{in} appears to be independent of the indentation condition used. The system with a smaller film thickness has a higher G_{in} value. The result is in good agreement with those measured by the monotonic loading dual-indentation method [9].

Cyclic and monotonic loading dual-indentations were performed on the SiN/GaAs systems with different interfaces shown in Table 1. Fig. 10 shows the average values of G_{in} calculated, together with their standard deviations. It is clear that for all the specimens being tested their G_{in} values obtained from the two approaches are in good agreement, with relatively small deviations, indicating the G_{in} values measured by the cyclic-loading indentation are reliable. It is also seen in Fig. 10 that the result for the Standard SiN specimens is only from the cyclic loading indentation as the monotonic loading indentation failed to generate delamination in this case. Accordingly, these specimens have the highest values of G_{in}.

5 Discussion

The indentation contact stress in malleable and strongly-adhered films tends to be consumed by plastic deformation rather than being transferred to elastic strain energy, which reduces the driving force for interfacial crack initiation and propagation [26, 27]. Among the five types of SiN films being studied, the Standard SiN films have the lowest hardness (see Table 2). During indentation these films were expected to experience the most plasticity, which could thus result in insufficient residual elastic strain energy to initiate interfacial delamination. Furthermore, as shown in Fig. 10 the G_{in} value of Standard SiN is the highest among all the systems examined. Thus, the malleability and better interfacial adhesion are believed to be

ACCEPTED MANUSCRIPT

accountable for the “well-adhered" behaviour of Standard SiN film subjected to normal monotonic loading indentation.

Our result demonstrated that cyclic loading indentation is an effective way to generate interfacial delamination to “well-adhered” film/substrate systems. In fact, cyclic indentation techniques have been used in a number of studies to delaminate film/substrate structures. For instance, Raju et al. [12, 13] used cyclic indentation to examine the interfacial delamination behaviour of TiN, AlN and SiC films. In their work indentation testing was repeated, with each cycle reloading to the maximum applied load. They demonstrated that a small amount of delamination in each loading cycle could be accumulated to a large extent. Cyclic indentation facilitated the extension of interfacial cracks through producing additional plastic deformation volume in both the film and substrate. In those studies, however, the measurement of the interfacial properties was not a concern. More recently, Wei et al. [14, 15] also used cyclic indentation to delaminate SiO_2/Si and diamond-like carbon/Si interfaces to determine G_{in}. Similar to Raju’s repeated load-unloading cycles, the sinusoidal cyclic oscillating loading used in their testing led to the propagation of interfacial delamination through the further penetration of indenter and inevitably the expansion of plastic deformation in the tested system. However, as the extension of interfacial cracks was proven to be supported through repeatedly applied load, the weakening of interface due to fatigue failure should be minimised. Therefore, in this study, gradually increased load was used in the cyclic indentation to reduce the plastic deformation.

To understand the delamination mechanism involved in the cyclic loading indentation, it is important to investigate the effect cyclic loading has on the mechanical properties of the SiN films, as well as their deformation behaviours. For this purpose, a set of cyclic loading indentations with different cycle numbers were performed on the Standard SiN films and their hardness, H, was calculated. In these tests, the indentation depth was controlled to be

ACCEPTED MANUSCRIPT

smaller than 10% of the film thickness so that the substrate effect was negligible. Fig. 11 shows the values of H and residual depth, h_f, obtained plotted as a function of the indentation cycles. It can be observed that H of the SiN films increases whilst the h_f decreases with the increase in indentation cycle. In fact, H increases from 12.7 GPa obtained by monotonic loading indentation to 13.45 GPa measured after 50 cycles of cyclic loading indentation, giving a rise of 5.3 %, while on the contrary h_f decreases from 56.2 nm to 49.7 nm, accounting for a 8.7% reduction. Fig. 12 summarizes the relative change in H, h_f as well as E between the monotonic and cyclic loading indentations for all the film/substrate systems studied. As can be seen, the rise of H is in the range of 3.8-7.3% while the reduction in h_f falls within 6.4% to 14.5%. In addition, an increase in E (0.5-1.7%) is also shown.

The hardening effect induced by imposed strain in amorphous/glassy materials has been previously reported [28-30]. Different from strain hardening in metallic materials, plastic deformation could lead to the densification of this amorphous PECVD silicon nitride [19, 31, 32] (as it is not fully dense) through clustering of vacancies, swapping and reordering of atoms. As a result, the plastically deformed region was often hardened. Increased hardness value and elastic modulus are often suggestive of a densification mechanism present in the tested amorphous films under indentation stress [33, 34]. It is thus likely that in this case cyclic loading generated more pronounced localized densification in the amorphous SiN films than monotonic-loading indentation, which thus resulted in the increased values of H and E (Fig. 12).

Fig. 13 illustrates the different deformation mechanisms of a malleable SiN film under monotonic and cyclic loading conditions. During monotonic loading, greater plastic deformation was produced in the SiN film and hence a greater penetration depth (h_m □ h_{m*}) was caused than the cyclic loading, as shown in Figs. 13(a) & (b). The substantial plastic deformation resulted in a more pronounced encroachment of the deformed SiN film

ACCEPTED MANUSCRIPT

conformed into the cavity formed due to the plastic deformation of the substrate. In this process, more generous strain energy was used in plastically bending the film towards the substrate and the residual elastic strain energy was thus insufficient to break the interfacial bonds. In the case of cyclic loading indentation, however, the indented SiN film was hardened, which impeded the plastic flow in the deforming SiN film (see Fig. 13(c)). More contact strain was thus stored in the flexed film in the forms of elastic strain energy in cyclic loading than monotonic loading. As a result, interfacial delamination was more likely initiated driven by the tensile stress being generated during unloading, attributed to the increased stored elastic strain energy in the flexed film, as shown in Fig. 13(d). As the energy released during incremental crack extension was independent of loading configuration, the calculated G_{in} remained unchanged regardless of the loading type used. This is supported by the evidence that the G_{in} values of all the film/substrate specimens being tested using cyclic loading dual-indentation are in excellent agreement with those obtained from the normal monotonic loading dual-indentation.

However, for the malleable SiN films, thickness reduction may be caused due to the encroachment of the SiN film into the deformed GaAs substrate. The inevitable "stretching" (both elastically and plastically) of the delaminated film may introduce error in the calculation of a using Eq. (6) and thus causes inaccuracy in the delamination area estimation. Nevertheless, as the deflections of the delaminated SiN films in this work were small in comparison with the film thicknesses, the error caused by thickness reduction due to plate stretching are expected to be insignificant. In fact, compared with monotonic loading indentation, cyclic loading indentation causes less plastic deformation in the SiN film, which may improve the accuracy in delamination area estimation.

Finally, it should be noted that the cyclic loading dual-indentation method proposed in this study can be used to replace the previous monotonic loading dual-indentation method, as the

ACCEPTED MANUSCRIPT

G_{in} values are in good agreement with those obtained from the previous method [9]. Also, this method was applicable to a larger variety of SiN/GaAs film/substrate systems than the monotonic loading method as it could measure the adhesion energies of films with tougher interfaces. Nevertheless, the monotonic loading method should be first considered as its testing protocol and data processing are much simpler. In addition, cyclic loading would cause additional wear to the indenter, particularly when dealing with hard films.

6 Conclusion

The cyclic loading dual-indentation method was developed to determine the interfacial energy release rate of the "well-adhered" SiN/GaAs film/substrate systems, in which monotonic loading dual-indentation was unable to generate interfacial delamination. The values of G_{in} determined by the cyclic loading method were in good agreement with those obtained from the monotonic loading indentation. The delamination mechanism involved was attributed to the hardening effect on the film caused by cyclic loading, which allowed more strain energy to be stored and thus provided extra driving force for interfacial delamination.

Acknowledgements

The authors would like to acknowledge the financial support of WIN Semiconductor Co. and Australian Research Council (ARC). This work was financially supported by ARC under the Future Fellow Program.

ACCEPTED MANUSCRIPT

Reference

[1] J.J. Chen, S.J. Bull, Approaches to investigate delamination and interfacial toughness in coated systems: an overview, J. Phys. D-Appl. Phys., 44 (2011) 034001.

[2] S.-Y. Chang, H.-C. Tsai, J.-Y. Chang, S.-J. Lin, Y.-S. Chang, Analyses of interface adhesion between porous SiOCH low-k film and SiCN layers by nanoindentation and nanoscratch tests, Thin Solid Films, 516 (2008) 5334-5338.

[3] K.B. Yeap, K.Y. Zeng, H.Y. Jiang, L. Shen, D.Z. Chi, Determining interfacial properties of submicron low-k films on Si substrate by using wedge indentation technique, J. Appl. Phys., 101 (2007) 123531.

[4] R.K. Singh, M.T. Tilbrook, Z.H. Xie, A. Bendavid, P.J. Martin, P. Munroe, M. Hoffman, Contact damage evolution in diamondlike carbon coatings on ductile substrates, J. Mater. Res., 23 (2008) 27-36.

[5] L.G. Rosenfeld, J.E. Ritter, T.J. Lardner, M.R. Lin, Use of the microindentation technique for determining interfacial fracture energy, J. Appl. Phys., 67 (1990) 3291-3296.

[6] A.A. Volinsky, N.R. Moody, W.W. Gerberich, Interfacial toughness measurements for thin films on substrates, Acta Mater., 50 (2002) 441-466.

[7] S. Zhang, Y.S. Wang, X.T. Zeng, K.A. Khor, W.J. Weng, D.E. Sun, Evaluation of adhesion strength and toughness of fluoridated hydroxyapatite coatings, Thin Solid Films, 516 (2008) 5162-5167.

[8] S. Zhang, X.M. Zhang, Toughness evaluation of hard coatings and thin films, Thin Solid Films, 520 (2012) 2375-2389.

[9] M. Lu, H. Huang, Determination of the energy release rate in the interfacial delamination of silicon nitride film on gallium arsenide substrate via nanoindentation, J. Mater. Res., 29 (2014) 801-810.

[10] M.D. Kriese, W.W. Gerberich, N.R. Moody, Quantitative adhesion measures of multilayer films: Part I. Indentation mechanics, J. Mater. Res., 14 (1999) 3007-3018.

ACCEPTED MANUSCRIPT

[11] A. Bagchi, G.E. Lucas, Z. Suo, A.G. Evans, A new procedure for measuring the decohesion energy for thin ductile films on substrates, J. Mater. Res., 9 (1994) 1734-1741.

[12] T. Dharma Raju, M. Kato, K. Nakasa, Backward deviation and depth recovery of load–displacement curves of amorphous SiC film under repeating nanoindentation, Acta Mater., 51 (2003) 3585-3595.

[13] T.D. Raju, K. Nakasa, M. Kato, Relation between delamination of thin films and backward deviation of load-displacement curves under repeating nanoindentation, Acta Mater., 51 (2003) 457-467.

[14] P.J. Wei, W.L. Liang, C.F. Ai, J.F. Lin, A new method for determining the strain energy release rate of an interface via force-depth data of nanoindentation tests, Nanotechnology, 20 (2009) 025701.

[15] P.J. Wei, S.B. Chio, W.L. Liang, J.F. Lin, Determining buckling strain energy release rate through indentation-induced delamination, Thin Solid Films, 519 (2011) 4889-4893.

[16] M. Lu, H. Xie, H. Huang, J. Zou, Y. He, Indentation-induced delamination of plasma-enhanced chemical vapor deposition silicon nitride film on gallium arsenide substrate, J. Mater. Res., 28 (2013) 1047-1055.

[17] W.C. Oliver, G.M. Pharr, Measurement of hardness and elastic modulus by instrumented indentation: Advances in understanding and refinements to methodology, J. Mater. Res., 19 (2004) 3-20.

[18] H. Huang, K. Winchester, Y. Liu, X.Z. Hu, C.A. Musca, J.M. Dell, L. Faraone, Determination of mechanical properties of PECVD silicon nitride thin films for tunable MEMS Fabry-Perot optical filters, J. Micromech. Microeng., 15 (2005) 608-614.

[19] H. Huang, K.J. Winchester, A. Suvorova, B.R. Lawn, Y. Liu, X.Z. Hu, J.M. Dell, L. Faraone, Effect of deposition conditions on mechanical properties of low-temperature PECVD silicon nitride films, Mater. Sci. Eng. A-Struct. Mater. Prop. Microstruct. Process., 435 (2006) 453-459.

ACCEPTED MANUSCRIPT

[20] Y.G. Jung, B.R. Lawn, M. Martyniuk, H. Huang, X.Z. Hu, Evaluation of elastic modulus and hardness of thin films by nanoindentation, J. Mater. Res., 19 (2004) 3076-3080.

[21] H. Xie, H. Huang, Characterization of the interfacial strength of SiNx/GaAs film/substrate systems using energy balance in nanoindentation, J. Mater. Res., 28 (2013) 3137-3145.

[22] S.V. Hainsworth, M.R. McGurk, T.F. Page, The effect of coating cracking on the indentation response of thin hard-coated systems, Surface and Coatings Technology, 102 (1998) 97-107.

[23] J. Chen, S.J. Bull, Indentation fracture and toughness assessment for thin optical coatings on glass, J. Phys. D-Appl. Phys., 40 (2007) 5401-5417.

[24] B.R. Lawn, Fracture of brittle solids, Cambridge University Press, New York, USA, 1993.

[25] S. Timoshenko, S. Woinowsky-Krieger, Theory of plates and shells, McGraw-Hill1959.

[26] A.A. Volinsky, J.B. Vella, W.W. Gerberich, Fracture toughness, adhesion and mechanical properties of low-K dielectric thin films measured by nanoindentation, Thin Solid Films, 429 (2003) 201-210.

[27] A. Abdul-Baqi, E. Van der Giessen, Indentation-induced interface delamination of a strong film on a ductile substrate, Thin Solid Films, 381 (2001) 143-154.

[28] D.M. Marsh, Plastic Flow in Glass, Proceedings of the Royal Society of London. Series A. Mathematical and Physical Sciences, 279 (1964) 420-435.

[29] G. Kermouche, E. Barthel, D. Vandembroucq, P. Dubujet, Mechanical modelling of indentation-induced densification in amorphous silica, Acta Mater., 56 (2008) 3222-3228.

[30] K.R. Gadelrab, F.A. Bonilla, M. Chiesa, Densification modeling of fused silica under nanoindentation, J. Non-Cryst. Solids, 358 (2012) 392-398.

ACCEPTED MANUSCRIPT

[31] H. Huang, X.Z. Hu, Y. Liu, M. Bush, K. Winchester, C. Musca, J. Dell, L. Faraone, Characterization of mechanical properties of silicon nitride thin films for MEMS devices by nanoindentation, J. Mater. Sci. Technol., 21 (2005) 13-16.

[32] V.-V. Le, T.-T. Nguyen, K.-H. Pham, The structural correlation and mechanical properties in amorphous silicon nitride under densification, J. Non-Cryst. Solids, 363 (2013) 6-12.

[33] R.A. Levy, X. Lin, J.M. Grow, H.J. Boeglin, R. Shalvoy, Low pressure chemical vapor deposition of silicon nitride using the environmentally friendly tris(dimethylamino)silane precursor, J. Mater. Res., 11 (1996) 1483-1488.

[34] N. Janakiraman, F. Aldinger, Indentation analysis of elastic and plastic deformation of precursor-derived Si–C–N ceramics, Journal of the European Ceramic Society, 30 (2010) 775-785.

ACCEPTED MANUSCRIPT

ACCEPTED MANUSCRIPT

Table list:

Table 1 Deposition conditions of the SiN film specimens

Sample description	Film thickness (nm)	SiH_4 flow rate (sccm)	NH_3 flow rate (sccm)	N_2 flow rate (sccm)	Depostion rate (Å/sec)	Temperature (°C)	System
Compressive SiN/GaAs	222 489 814	300	600	4900	60.5	250	Trikon
DL-com $SiNGaA_S$	207 495 787	285	1000	1000	25.5	300	Novellus
Dense SiN/GaA_S	215 523 843	5	3	1800	2.4	250	Trikon
Cap SiN/GaA_S	227 530 842	260	1700	1040	10	300	Novellus
Standard SiN/GaA_S	182 520 823	125	250	1800	4.9	250	Trikon
GaAs wafer	GaAs wafers are approximately 660 μm thick in finished product						

ACCEPTED MANUSCRIPT

ACCEPTED MANUSCRIPT

Table 2 Elastic modulus *E* and hardness *H* of the SiN films and the GaAs substrate

Films	*E* (GPa)	*H* (GPa)
Compressive	152.1	17.2
DL-com	133.2	15.1
Dense	148.2	15.7
Cap	156	16.8
Standard	115.4	12.7
GaAs	120.6	8.03

ACCEPTED MANUSCRIPT

ACCEPTED MANUSCRIPT

Table 3 Energy release rate G_{in} derived from monotonic-loading and cyclic-loading dual-indentations

Films	Thickness (nm)	G_{in} (J/m^2)	
		Static-loading	Cyclic-loading
Compressive	222	2.59±0.28	2.32±0.32
	489	1.6±0.12	1.87±0.12
	814	0.76±0.09	0.78±0.09
DL-com	207	2.19±0.07	2.1±0.39
	495	0.98±0.11	0.91±0.1
	787	0.65±0.09	0.67±0.07

ACCEPTED MANUSCRIPT

ACCEPTED MANUSCRIPT

Figure list:

Fig. 1 The load functions of (a) cyclic loading and (b) monotonic loading dual-indentations.

Fig. 2 The flow chart of the energy-based method for the evaluation of interfacial energy release rate.

Fig. 3 Illustration of the energy calculation for indentation-induced delamination [9].

Fig. 4 The centrally loaded clamped circular plate model for delamination area estimation [9].

Fig. 5 (a) Typical *P-h* curve of a cyclic indentation (33 cycles) and (b) the enlarged image of the area marked in the dashed rectangle in (a), showing the 2nd derivative of the final indent loading portion and the curve fitting result using Hertz elastic contact theory.

Fig. 6 The G_{in} values plotted against the indentation cycle number. The Compressive SiN film used was 222 nm in thickness, the maximum load was 7 mN. Each data point are the average value of 18 indents.

Fig. 7 The *P-h* curves of a single and a cyclic (33 cycles) indentations. The Standard SiN film used was 180 nm in thickness, the maximum load was 8 mN.

Fig. 8 The occurrence of delamination plotted against the number of cycles. The Standard SiN film was 520 nm in thickness, the maximum load was 22 mN. For each cycle number 18 indents were made.

Fig. 9 (a) Delamination energy U_s and (b) interfacial energy release rate G_{in} of the Standard SiN films of various thicknesses obtained from the (33 cycles) cyclic loading dual-indentation.

Fig. 10 Comparison of the energy release rates obtained from the monotonic loading and the cyclic loading dual-indentations. The values inside the plots represent the film's thicknesses.

Fig. 11 The hardness H and residual depth h_f of the Standard SiN film plotted as a function of the number of cycles. The film thickness was 823 nm and the maximum load was 7 mN. Each data point are the average value of 9 indents.

ACCEPTED MANUSCRIPT

Fig. 12 The relative difference (in percentage) in hardness H, residual depth h_f and elastic modulus E between the values measured using monotonic loading indentation and cyclic loading indentation. The film thicknesses were around 800 nm and the maximum load was 7 mN.

Fig. 13 Schematic illustration showing different deformation behaviour under different loading conditions: (a) monotonically loading till maximum load is reached; (b) film remains attached to the substrate after monotonic loading indentation; (c) cyclically loading till maximum load is reached; (d) interfacial delamination under cyclic-loading indentation.

ACCEPTED MANUSCRIPT

ACCEPTED MANUSCRIPT

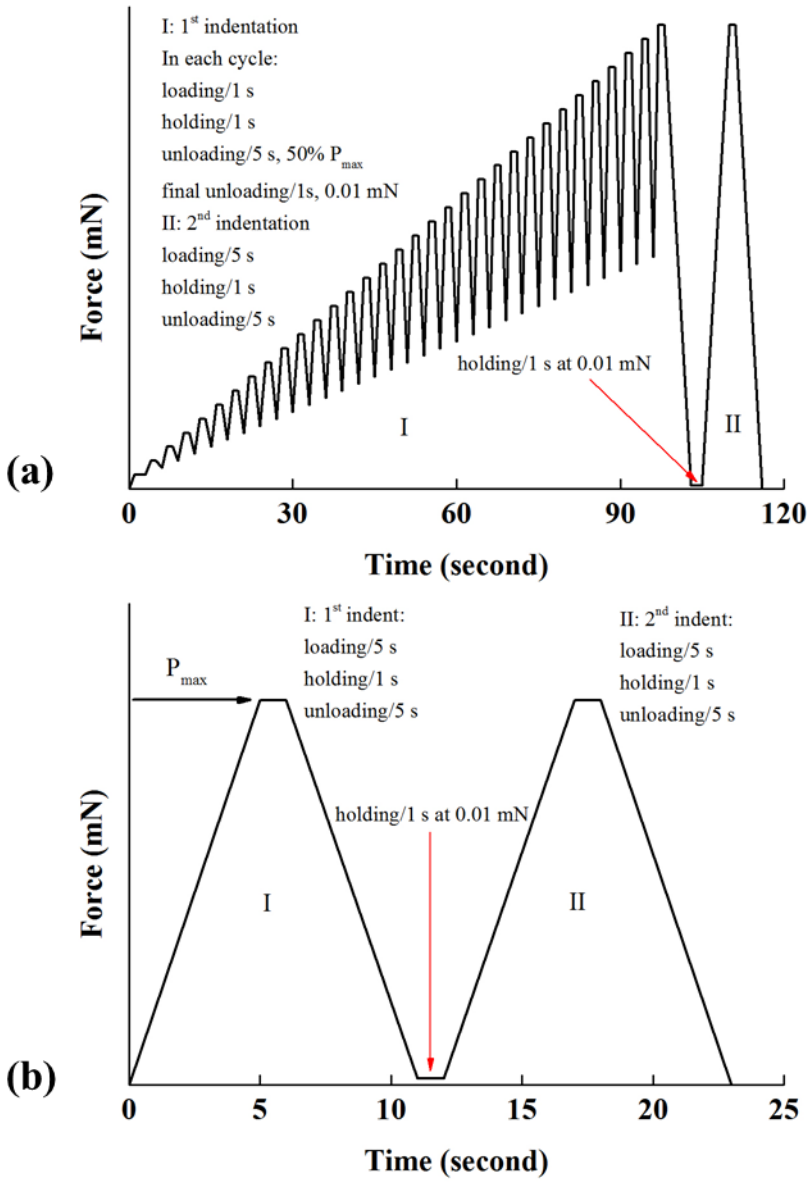

Figure 1

ACCEPTED MANUSCRIPT

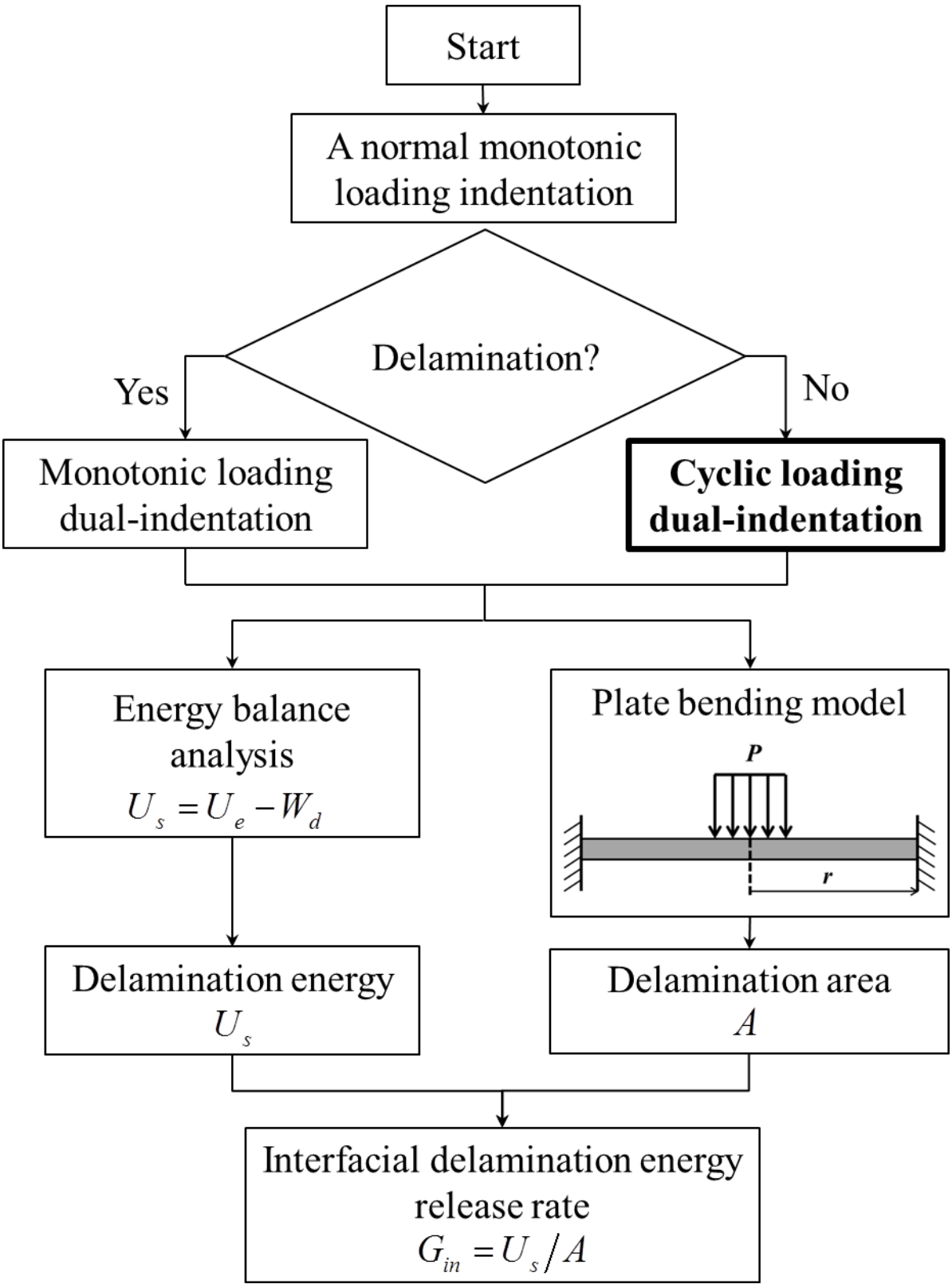

Figure 2

ACCEPTED MANUSCRIPT

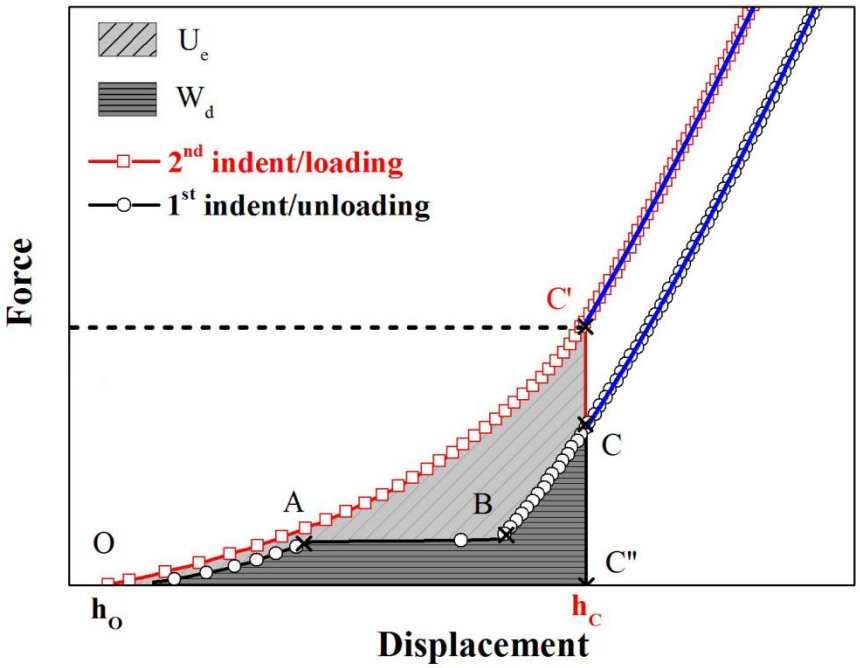

Figure 3

ACCEPTED

ACCEPTED MANUSCRIPT

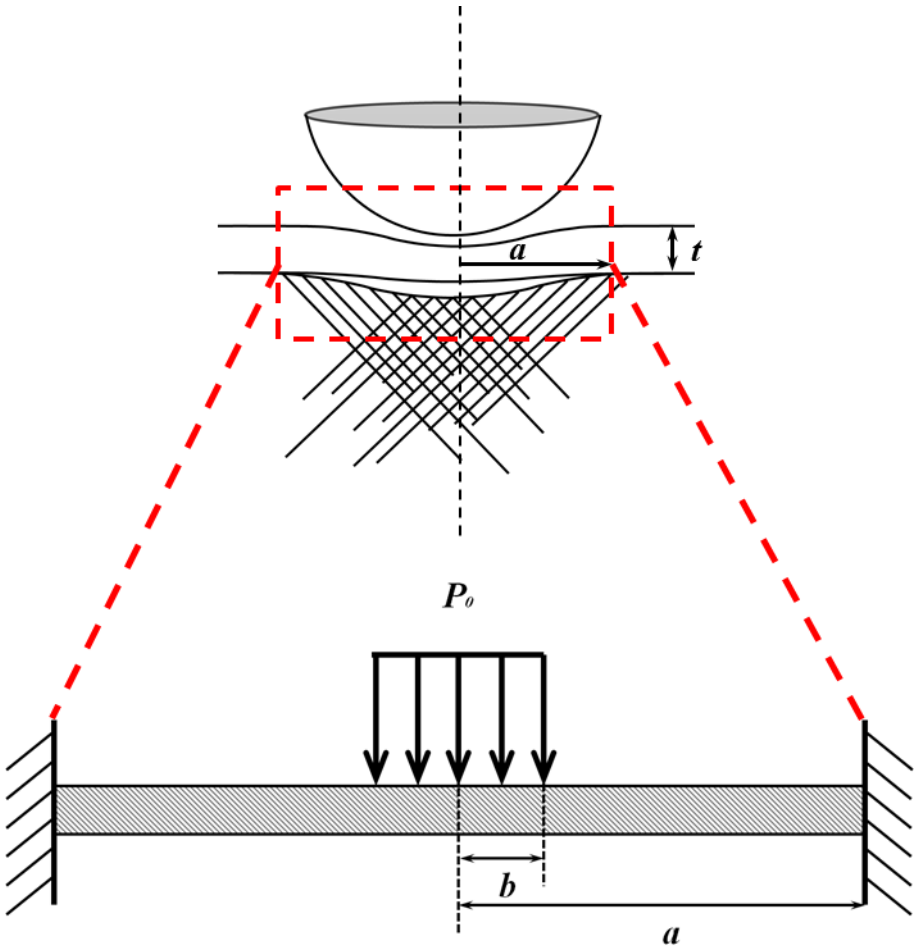

Figure 4

ACCEPT

ACCEPTED MANUSCRIPT

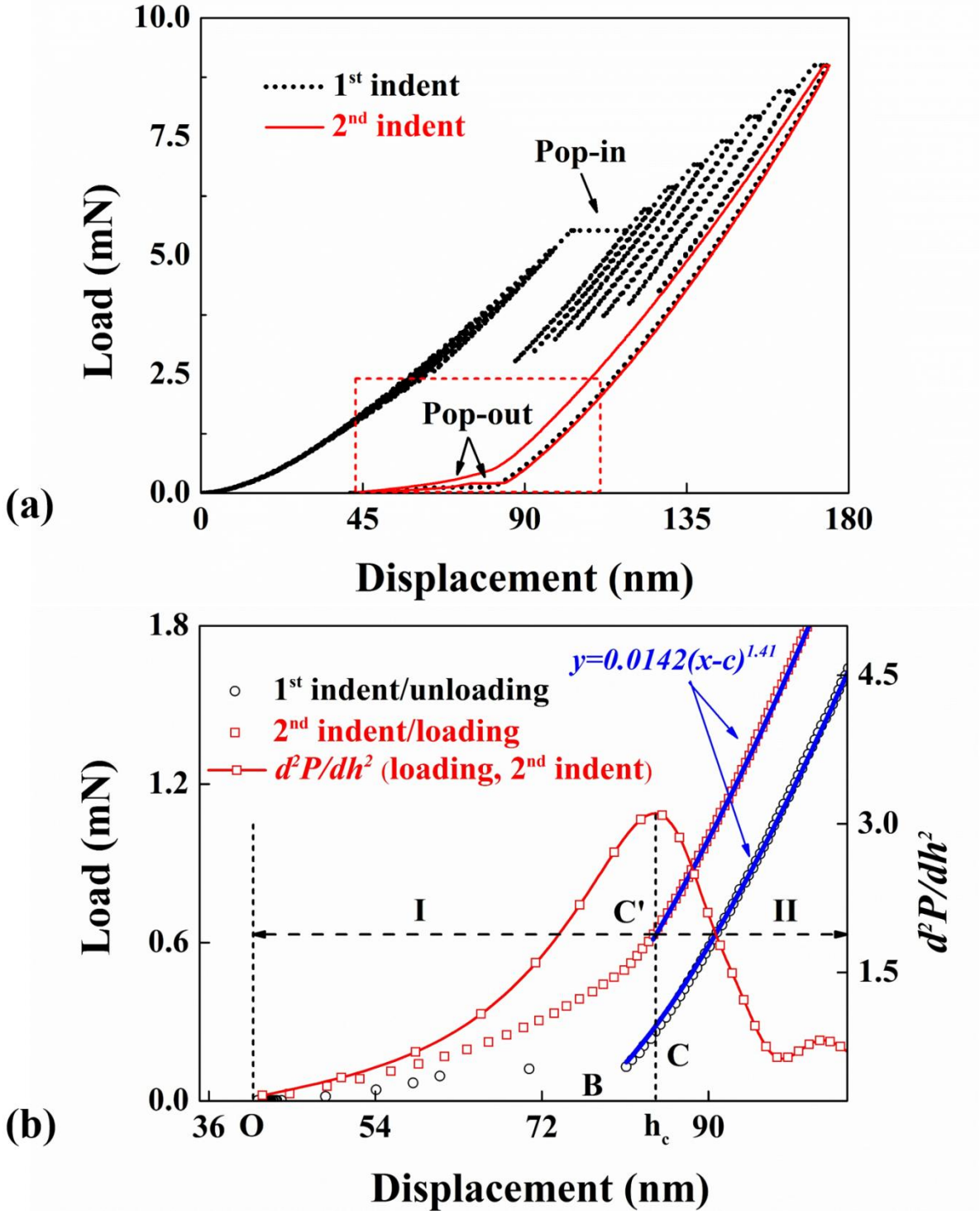

Figure 5

ACCEPTED MANUSCRIPT

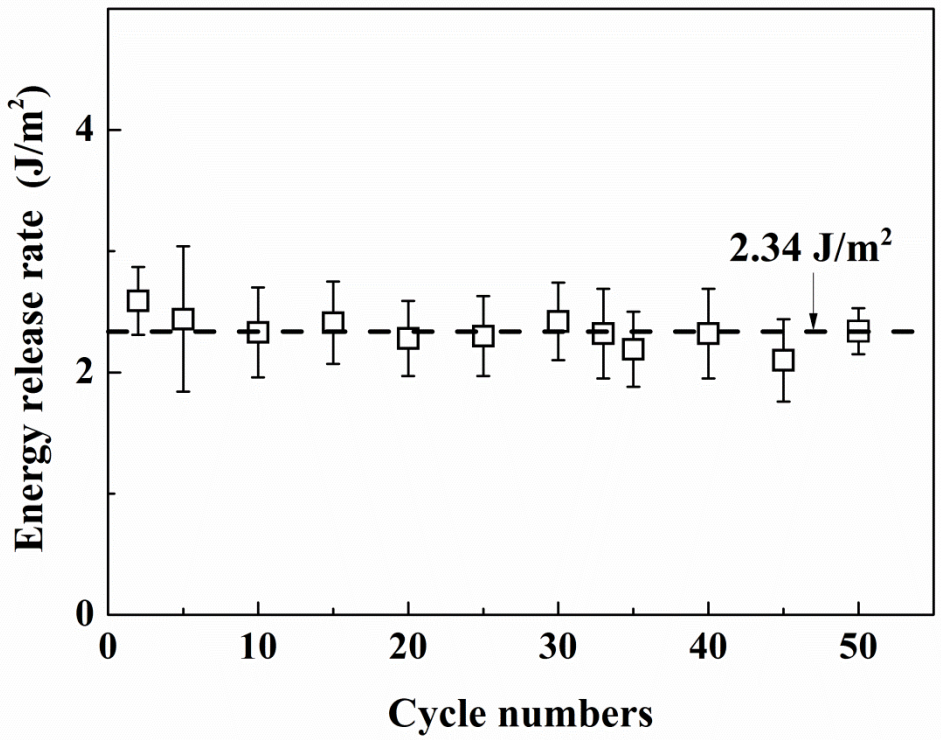

Figure 6

ACCEPTED

ACCEPTED MANUSCRIPT

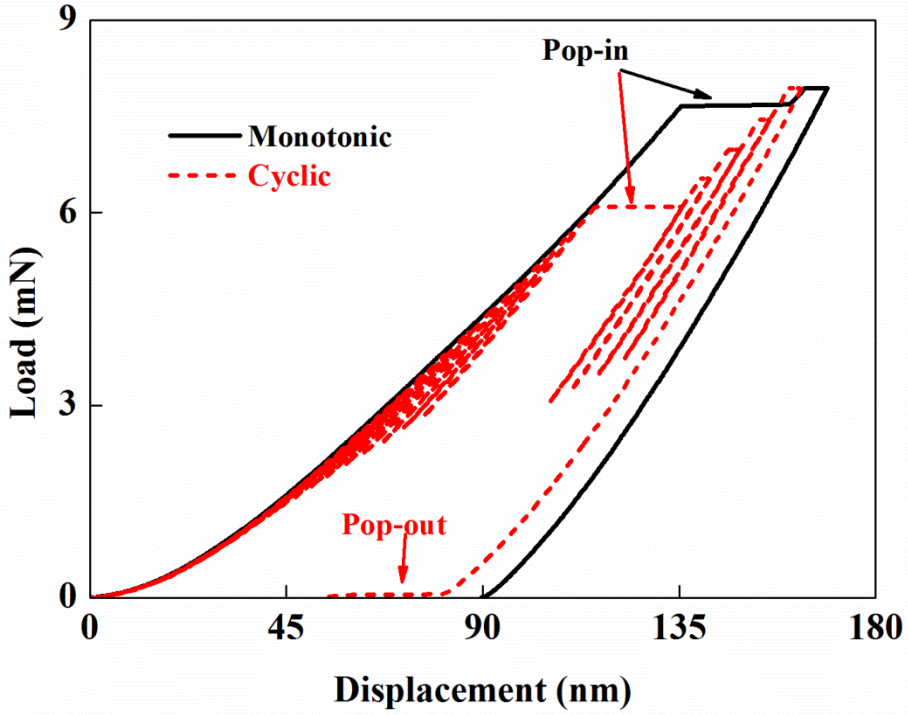

Figure 7

ACCEPTED

ACCEPTED MANUSCRIPT

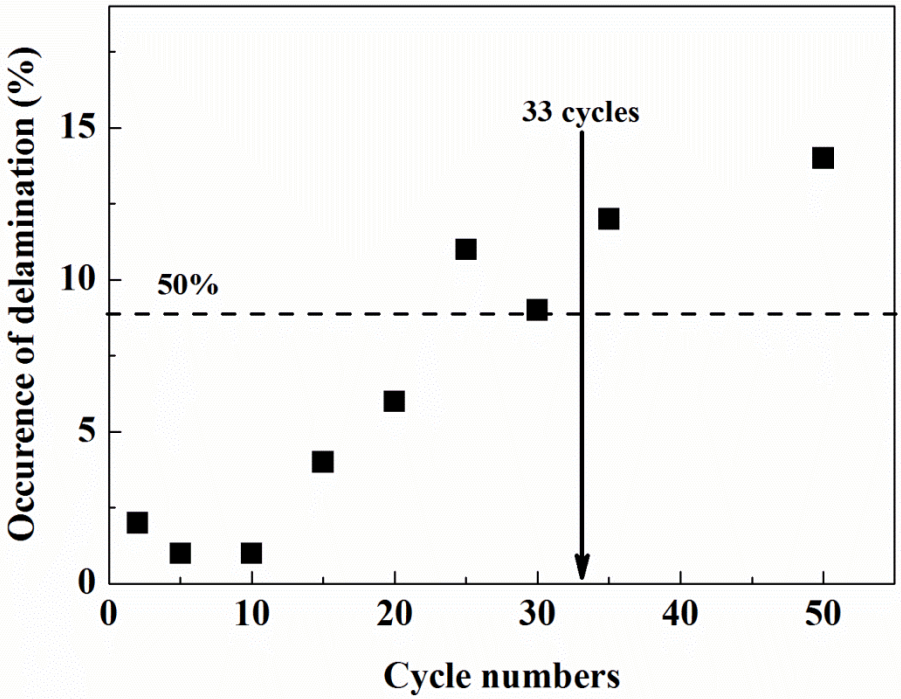

Figure 8

ACCEPTED MANUSCRIPT

ACCEPTED MANUSCRIPT

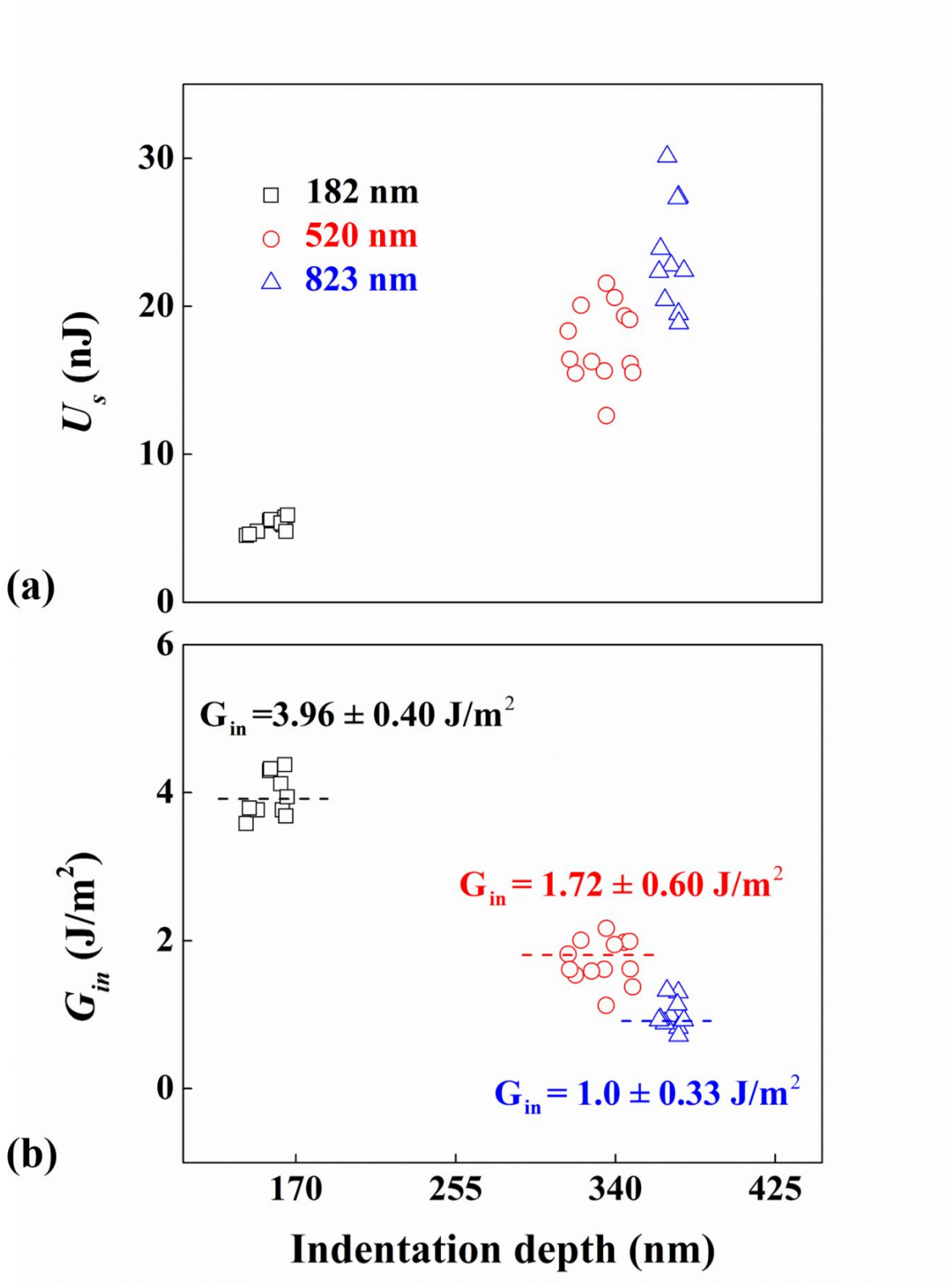

Figure 9

ACCEPTED MANUSCRIPT

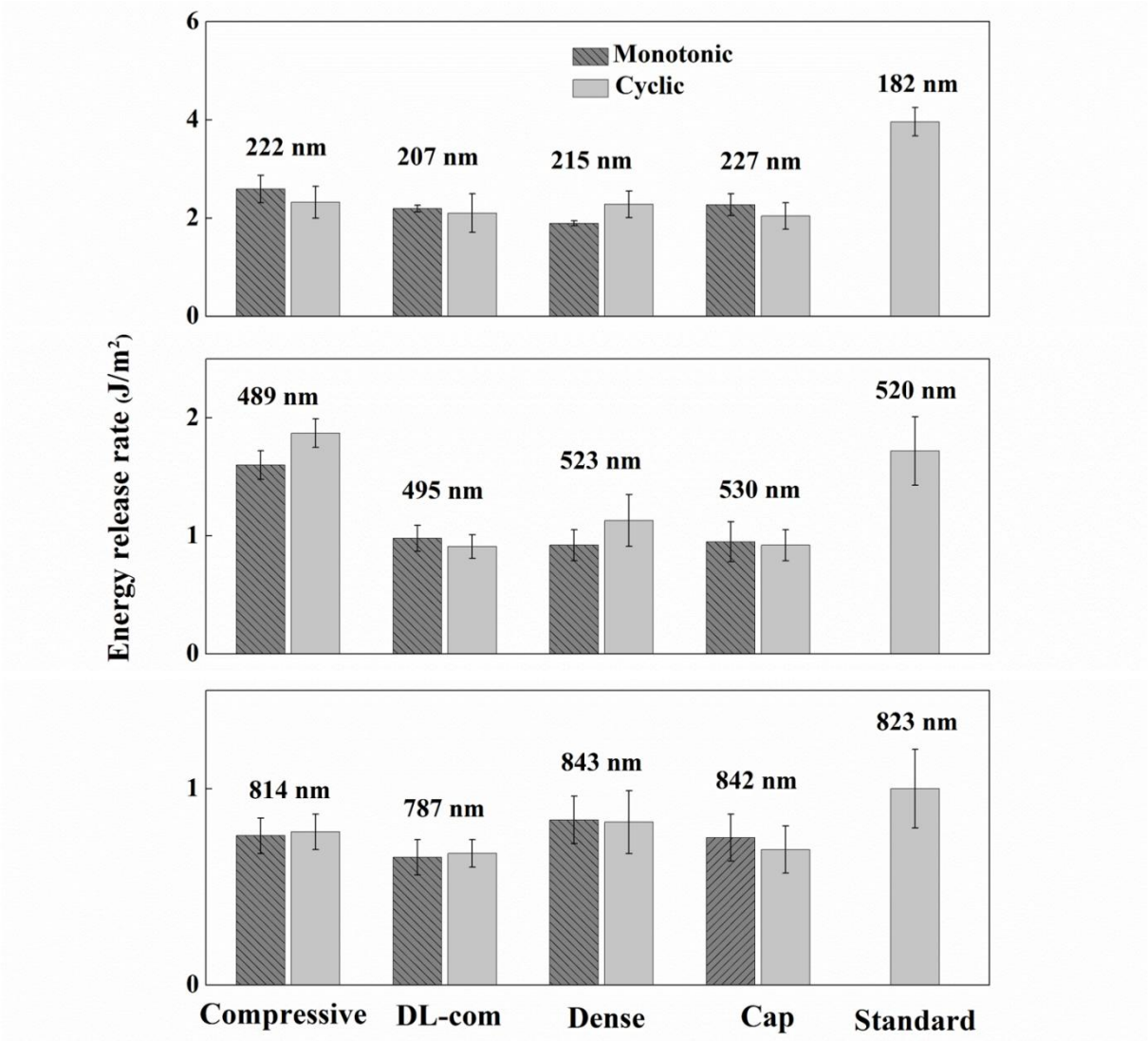

Figure 10

ACCEPTED

ACCEPTED MANUSCRIPT

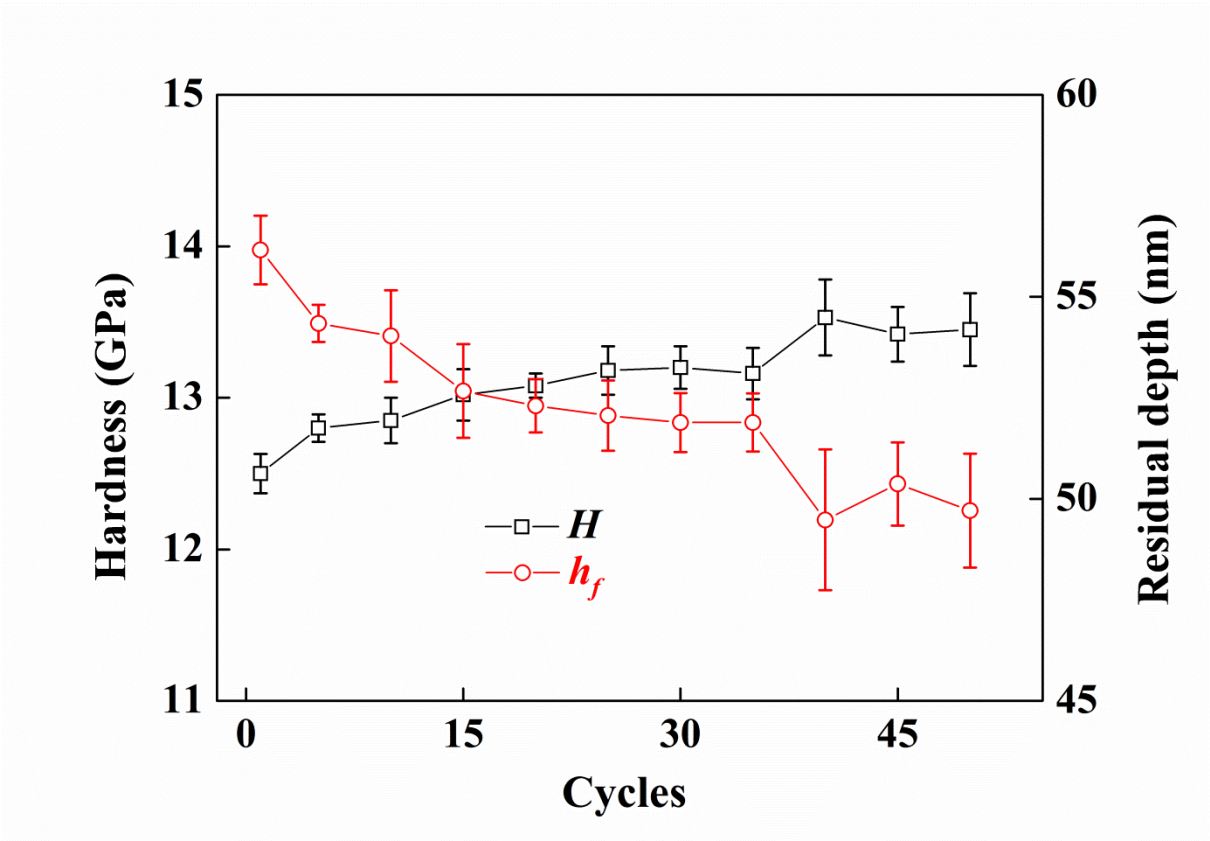

Figure 11

ACCEPTED

ACCEPTED MANUSCRIPT

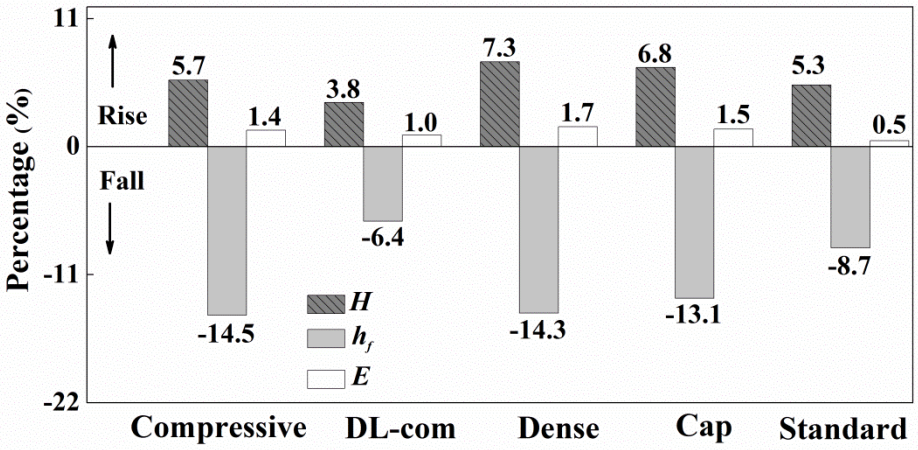

Figure 12

ACCEPTED MANUSCRIPT

ACCEPTED MANUSCRIPT

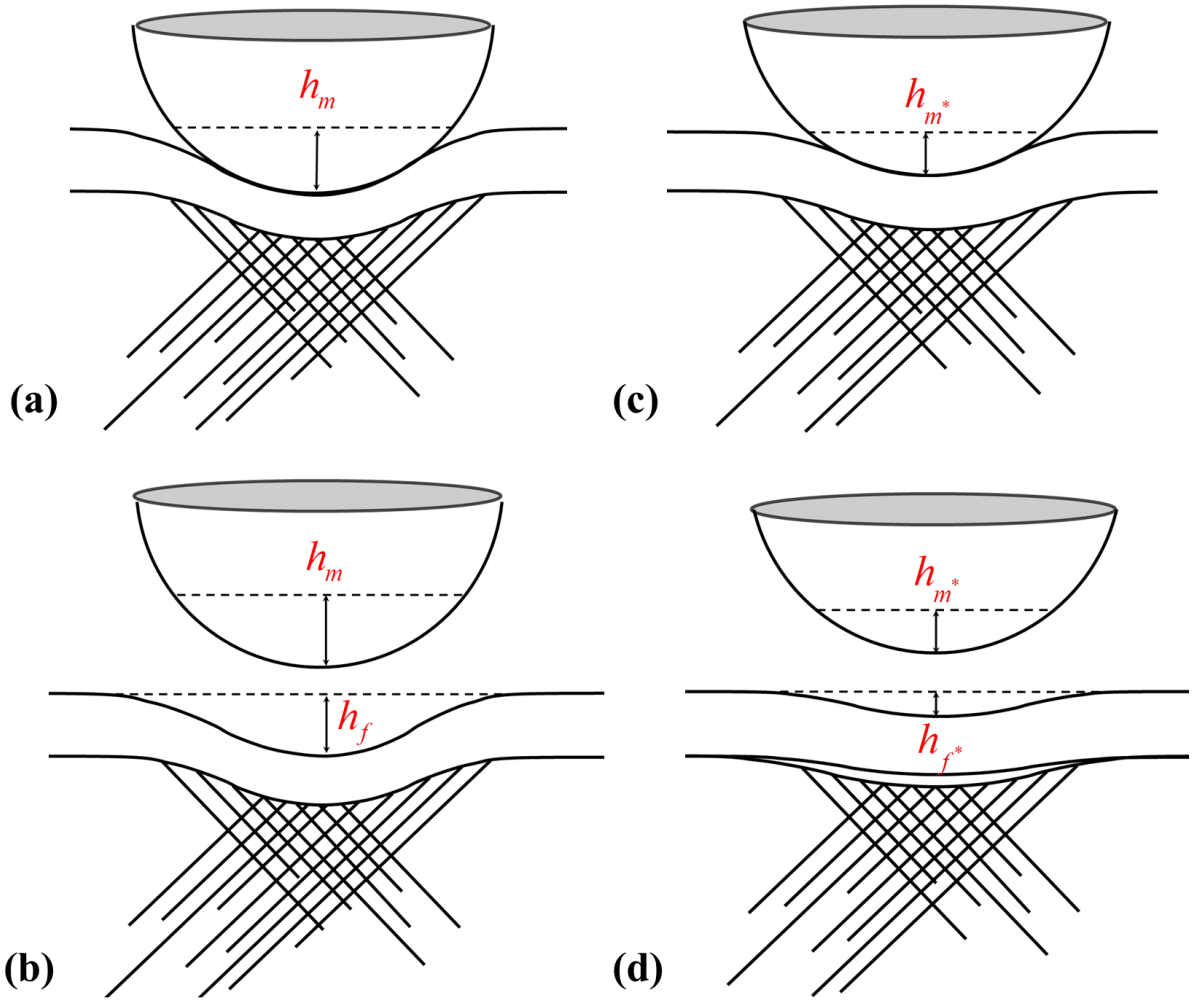

Figure 13

ACCEPT

ACCEPTED MANUSCRIPT

Highlights

- Cyclic-loading dual-indentation for measuring interfacial adhesion
- Breaking the “tough” interface without weakening the interfacial property
- Hardening effect on the indented film induced by cyclic loading
- Stored elastic energy in the hardened film drives delamination

ACCEPTED MANUSCRIPT